Available online at www.sciencedirect.com
SCIENCE DIRECT®
ELSEVIER
International Journal of Solids and Structures 42 (2005) 4058–4076
INTERNATIONAL JOURNAL OF SOLIDS and STRUCTURES
www.elsevier.com/locate/ijsolstr

Kinematic limit analysis of frictional materials using nonlinear programming

H.X. Li, H.S. Yu *

School of Civil Engineering, The University of Nottingham, University Park, Nottingham NG7 2RD, UK

Received 25 November 2004
Available online 21 January 2005

Abstract

In this paper, a nonlinear numerical technique is developed to calculate the plastic limit loads and failure modes of frictional materials by means of mathematical programming, limit analysis and the conventional displacement-based finite element method. The analysis is based on a general yield function which can take the form of the Mohr–Coulomb or Drucker–Prager criterion. By using an associated flow rule, a general nonlinear yield criterion can be directly introduced into the kinematic theorem of limit analysis without linearization. The plastic dissipation power can then be expressed in terms of kinematically admissible velocity fields and a nonlinear optimization formulation is obtained. The nonlinear formulation only has one constraint and requires considerably less computational effort than a linear programming formulation. The calculation is based entirely on kinematically admissible velocities without calculation of the stress field. The finite element formulation of kinematic limit analysis is developed and solved as a nonlinear mathematical programming problem subject to a single equality constraint. The objective function corresponds to the plastic dissipation power which is then minimized to give an upper bound to the true limit load. An effective, direct iterative algorithm for kinematic limit analysis is proposed in this paper to solve the resulting nonlinear mathematical programming problem. The effectiveness and efficiency of the proposed method have been illustrated through a number of numerical examples.

Keywords: Limit analysis; Frictional materials; Nonlinear programming; Upper bound analysis; Finite element method

* Corresponding author. Tel.: +44 115 8466884; fax: +44 115 9513898.
E-mail address: hai-sui.yu@nottingham.ac.uk (H.S. Yu).

0020-7683/$ - see front matter © 2005 Elsevier Ltd. All rights reserved.
doi:10.1016/j.ijsolstr.2004.11.023

1. Introduction

To obtain the stability condition and the maximum load of a structure under static loading, a step-by-step method based on traditional elastic-plastic analysis is commonly used. However, this incremental approach is often too cumbersome to use in practice because it requires a complete specification of the stress–strain relation and the nonlinear material properties of a structure. Therefore, other direct methods of stability analysis, such as the slip line method, limit equilibrium method and limit analysis, have been developed and applied to determine the plastic limit state of a continuous media directly (Chen, 1975). The slip line analysis, commonly used in metal forming processes under the plane strain condition, helps to find the stresses at the plastic state by satisfying a yield criterion and local equilibrium equations. Therefore, the slip line method is usually used for the stability analysis under the plane strain condition. In order to use the limit equilibrium method, a failure surface is usually assumed to be of a simple type (e.g., a plane, a circle or a logspirale). This would reduce the difficulty in seeking the position of critical surfaces for sliding or collapse.

Limit analysis is a rigorous and powerful solution method to the stability problem of structures. It can be used to calculate plastic limit loads of a structure in a direct way and provides a theoretical foundation for the engineering design and integrity assessment of structures. The limit analysis is based on two dual theorems, the static theorem (or the lower bound theorem) and the kinematic theorem (or the upper bound theorem). Due to the complexity of engineering problems, it is difficult to obtain an analytical solution and numerical techniques are usually required for limit analysis. Over the last three decades, many studies have been devoted to developing numerical methods of limit analysis. The finite element method has been widely used in limit analysis with the aid of mathematical programming techniques. In particular, a linear technique (e.g., Maier, 1969; Lysmer, 1970; Turgeman and Pastor, 1982; Sloan, 1988; Yu and Sloan, 1994; Yu et al., 1994; Sloan and Kleeman, 1995; Yu and Sloan, 1997; Francescato and Pastor, 1997) based on the programming theory was first used to conduct numerical limit analysis, where convex yield surfaces were linearized to obtain a linear programming problem. Although it is not very difficult to solve this type of linear problems, the linearization of a yield surface introduces a large number of constraints and it increases the computational cost. Based on the elastic compensation method, Ponter and Carter (1997, 2000, 2002) recently developed a linear numerical technique (termed as the Linear Matching Method) to perform kinematic limit analysis. The linear solutions are defined with a spatially varying shear modulus which provides a sequence of upper bounds to the limit load.

Following the work of Zouain et al. (1993), Lyamin and Sloan (2002a,b) presented a nonlinear numerical method to perform kinematic and static limit analyses by means of linear finite elements and nonlinear programming. The collapse load can be calculated by solving a nonlinear programming problem subject to a number of equality and inequality constraints. The objective function corresponding to the dissipated power is expressed in terms of both stresses and velocities. Velocity and stress discontinuities are used in these formulations. Therefore, additional constraints will have to be enforced on the nodal velocities or the nodal stresses. A potential difficulty in applying these formulations is that special stress or displacement finite elements need to be used.

An alternative nonlinear technique (Zhang et al., 1991; Liu et al., 1995; Zhang and Lu, 1995; Chen et al., 1998; Li et al., 2001, 2003; Capsoni et al., 2001), which is based on the nonlinear programming theory, has been used with much success to perform limit analysis of non-frictional materials. By using an associated flow rule, yield criteria can be directly introduced into the bound theorems of limit analysis without linearization. A nonlinear programming problem, subject to a small number of constraints, can be obtained for calculating the plastic collapse. In conjunction with the conventional finite element method, limit analysis can then be easily performed for a structure. This method has the advantages of good accuracy and modest computational effort. Up to now, however, this approach has only been applied for von Mises yield criterion (Zhang et al., 1991; Liu et al., 1995; Zhang and Lu, 1995; Chen et al., 1998; Li et al., 2003) and Hill's yield criterion (Li et al., 2001; Capsoni et al., 2001).

The objective of this paper is to extend the latter nonlinear technique so that it can be used to calculate plastic collapse loads of frictional materials obeying either the Mohr–Coulomb or Drucker–Prager yield criterion. The failure modes of a structure can also be obtained by the proposed upper bound method. The kinematic approach of limit analysis consists of minimising the plastic dissipation power throughout a rigid perfectly plastic body. By using a general yield criterion and the associated flow rule, the plastic dissipation power can be expressed in terms of a kinematically admissible velocity field. Based on the nonlinear programming theory, the finite element modelling of kinematic limit analysis for the frictional materials is formulated as a nonlinear mathematical programming problem subject to a single equality constraint. The nondifferentiability of the objective function may lead to numerical difficulties in solving the nonlinear programming problem. A penalization factor is therefore proposed to overcome the numerical difficulty caused by the non-differentiability of the objective function. Then a direct iterative algorithm is developed for solving the nonlinear mathematical programming problem.

A main task in performing a kinematic limit analysis for frictional materials is to implement a nonlinear yield criterion into the kinematic theorem of limit analysis, because this criterion is expressed by a polynomial with both first and second degree terms. This potential difficulty has been successfully overcome in this paper. The objective function corresponding to the dissipation power is expressed in terms of a kinematically admissible velocity field. The stress field within the body does not need to be calculated and the limit state of a structure can be obtained. This will significantly reduce the required computational effort. The yield surface is not linearized and this can greatly decrease the number of constraints and the computational effort. The nonlinear mathematical programming problem is only subject to a small number of equality constraints which can be easily solved by the algorithm in this paper. Numerical experiments and results illustrate the high efficiency, low computational effort and good numerical stability of the proposed algorithm.

2. Limit analysis based on a general yield criterion

In limit analysis, it is assumed that the deformation is small at incipient collapse and the material can be modelled with sufficient accuracy using rigid, perfect plasticity and an associated flow rule. For soil materials, most yield criteria are expressed by a polynomial with both first and second degree terms to describe the effect of hydrostatic pressure on the yield of materials (e.g. the Mohr–Coulomb and Drucker–Prager criteria). It is quite difficult to directly introduce these criteria into the plastic limit analysis. A numerical technique based on the nonlinear mathematical programming will be developed to perform kinematic limit analysis for these yield criteria. Note that a tensile stress is assumed to be positive in this paper. Moreover, in order to use the finite element method, we adopt column vectors to represent strains and stresses. For example, in a 2-dimensional model, $\boldsymbol{\varepsilon} = [\varepsilon_{11}, \varepsilon_{22}, 2\varepsilon_{12}]^{\mathrm{T}}$, and $\boldsymbol{\sigma} = [\sigma_{11}, \sigma_{22}, \sigma_{12}]^{\mathrm{T}}$, and in a 3-dimensional model, $\boldsymbol{\varepsilon} = [\varepsilon_{11}, \varepsilon_{22}, \varepsilon_{33}, 2\varepsilon_{12}, 2\varepsilon_{23}, 2\varepsilon_{31}]^{\mathrm{T}}$, and $\boldsymbol{\sigma} = [\sigma_{11}, \sigma_{22}, \sigma_{33}, \sigma_{12}, \sigma_{23}, \sigma_{31}]^{\mathrm{T}}$.

2.1. A general yield criterion

Many widely used yield criteria for frictional materials can be expressed in a general form as follows:

$$F(\boldsymbol{\sigma}) = \boldsymbol{\sigma}^{\mathrm{T}}\boldsymbol{P}\boldsymbol{\sigma} + \boldsymbol{\sigma}^{\mathrm{T}}\boldsymbol{Q} - 1 = 0 \tag{1}$$

where $F(\boldsymbol{\sigma})$ defines a yield function in terms of strength parameters, $\boldsymbol{P}$ and $\boldsymbol{Q}$ are coefficient vectors and related to the strength properties of the material.

The expression (1) can be regarded as a general yield criterion for frictional materials. For example, the Mohr–Coulomb criterion in plane strain can be expressed as

$$F(\sigma_{ij}) = (\sigma_{xx} - \sigma_{yy})^2 + (2\sigma_{xy})^2 - (2c\cos\varphi - (\sigma_{xx} + \sigma_{yy})\sin\varphi)^2 = 0 \tag{2}$$

where c and φ are the cohesion and the internal friction angle of the material respectively. It can be shown that the Mohr–Coulomb criterion can be expressed in the form of Eq. (1) with the following relations:

$$\boldsymbol{P} = \begin{bmatrix} \frac{1}{4c^2} & \frac{-1-\sin^2\varphi}{4c^2\cos^2\varphi} & 0 \\ \frac{-1-\sin^2\varphi}{4c^2\cos^2\varphi} & \frac{1}{4c^2} & 0 \\ 0 & 0 & \frac{1}{c^2\cos^2\varphi} \end{bmatrix} \tag{3}$$

$$\boldsymbol{Q} = \begin{bmatrix} \frac{\sin\varphi}{c\cos\varphi} \\ \frac{\sin\varphi}{c\cos\varphi} \\ 0 \end{bmatrix} \tag{4}$$

The Drucker–Prager criterion is also frequently used for frictional materials and can be expressed as

$$F(\sigma) = \varphi_0 I_1 + \sqrt{J_2} - c_0 = 0 \tag{5}$$

where I_1 is the first invariant of stress tensor, J_2 is the second invariant of the deviatoric stress tensor, φ_0 and c_0 are strength parameters of the material. In a general stress state, Eq. (1) can also be used to define the Drucker–Prager criterion under the following conditions:

$$\boldsymbol{P} = \begin{bmatrix} \frac{1-3\varphi_0^2}{3c_0^2} & -\frac{1+6\varphi_0^2}{6c_0^2} & -\frac{1+6\varphi_0^2}{6c_0^2} & 0 & 0 & 0 \\ -\frac{1+6\varphi_0^2}{6c_0^2} & \frac{1-3\varphi_0^2}{3c_0^2} & -\frac{1+6\varphi_0^2}{6c_0^2} & 0 & 0 & 0 \\ -\frac{1+6\varphi_0^2}{6c_0^2} & -\frac{1+6\varphi_0^2}{6c_0^2} & \frac{1-3\varphi_0^2}{3c_0^2} & 0 & 0 & 0 \\ 0 & 0 & 0 & \frac{1}{c_0^2} & 0 & 0 \\ 0 & 0 & 0 & 0 & \frac{1}{c_0^2} & 0 \\ 0 & 0 & 0 & 0 & 0 & \frac{1}{c_0^2} \end{bmatrix} \tag{6}$$

$$\boldsymbol{Q} = \begin{bmatrix} \frac{2\varphi_0}{c_0} & \frac{2\varphi_0}{c_0} & \frac{2\varphi_0}{c_0} & 0 & 0 & 0 \end{bmatrix}^{\mathrm{T}} \tag{7}$$

2.2. Kinematic theorem of limit analysis

An upper bound to the plastic limit load of a structure can be obtained by using the kinematic theorem of limit analysis (Drucker, 1953). The kinematic theorem states: among all kinematically admissible velocities, the real one yields the lowest rate of plastic dissipation power. Because the kinematic theorem is based on the concept of an admissible plastic strain rate, it can be formulated as

$$\lambda \int_{\Gamma_\sigma} t_i u_i^* \mathrm{d}\Gamma \leqslant \int_V D(\varepsilon_{ij}^*)\mathrm{d}v - \int_V f_i u_i^* \mathrm{d}v \tag{8}$$

where λ is the limit load multiplier, t_i is the basic load of surface tractions, f_i is the body force, u_i^* is the displacement velocity vector, ε_{ij}^* is the strain rate tensor, $D(\varepsilon_{ij}^*)$ denotes the function for the rate of the plastic dissipation power in terms of the admissible strain rate ε_{ij}^*, the superscript "*" stands for parameters corresponding to kinematically admissible fields, Γ_σ denotes the traction boundary and V denotes the space domain of the structure.

The rate of plastic dissipation power is defined by

$$D(\varepsilon_{ij}) = \sigma_{ij}\varepsilon_{ij} \tag{9}$$

According to mathematical programming theory, the kinematic theorem (8) can be revised as the following formulation if the internal body force is omitted:

$$\begin{cases} \lambda = \min \int_V \sigma_{ij}\varepsilon_{ij}\mathrm{d}v \\ \text{s.t.} \quad \int_{\Gamma_\sigma} t_i u_i \mathrm{d}\Gamma = 1 \\ \qquad \varepsilon_{ij} = \frac{1}{2}(u_{i,j} + u_{j,i}) \quad \text{in } V \\ \qquad u_i = 0 \qquad\qquad\quad \text{on } \Gamma_u \end{cases} \tag{10}$$

where "s.t." is the abbreviation of "subject to" and Γ_u denotes the displacement boundary. Thus, the kinematic limit analysis of a structure is finally reduced to the calculation of the limit load multiplier λ with λt_i denoting the limit load of the structure.

2.3. Dissipation power for a general yield criterion

Considering that the kinematic limit analysis is based on displacement modes, the stress terms need to be replaced by the strain terms, i.e., the dissipation power per unit volume in Eq. (10) should be expressed in terms of strain fields which can be obtained by using the yield criterion of a material and an plastic flow rule. The plastic flow rule determines the direction of the plastic strain rate vector by the following normality relation:

$$\dot{\varepsilon}_{ij}^p = \dot{\mu}\frac{\partial\phi(\sigma_{ij})}{\partial\sigma_{ij}} \tag{11}$$

where $\phi(\sigma_{ij})$ denotes a plastic potential function that resembles the yield function and $\dot{\mu}$ is a non-negative plastic proportionality factor. In the theory of limit analysis, the flow rule is assumed to be associative, i.e. $\phi(\sigma_{ij}) = F(\sigma_{ij})$. Hence the plastic strain rate can be expressed as

$$\boldsymbol{\varepsilon} = 2\mu\boldsymbol{P}\boldsymbol{\sigma} + \mu\boldsymbol{Q} \tag{12}$$

Therefore, the stress vector at the yield surface can be expressed in terms of the strain rate vector using the following formulation

$$\boldsymbol{\sigma} = \frac{1}{2\mu}\boldsymbol{P}^{-1}\boldsymbol{\varepsilon} - \frac{1}{2}\boldsymbol{P}^{-1}\boldsymbol{Q} \tag{13}$$

When the matrix $\boldsymbol{P}$ is non-singular, $\boldsymbol{P}^{-1}$ can be uniquely determined. However, if the matrix $\boldsymbol{P}$ is singular, we can use $(\boldsymbol{P} + \gamma\delta)^{-1}$ as an approximation for $\boldsymbol{P}^{-1}$, where γ is a small real number ($\gamma \to 0$).

By introducing Eq. (13) into the yield criterion (1), the following calculation can be obtained

$$\begin{aligned} \boldsymbol{\sigma}^{\mathrm{T}}\boldsymbol{P}\boldsymbol{\sigma} + \boldsymbol{\sigma}^{\mathrm{T}}\boldsymbol{Q} &= \left(\frac{1}{2\mu}\boldsymbol{P}^{-1}\boldsymbol{\varepsilon} - \frac{1}{2}\boldsymbol{P}^{-1}\boldsymbol{Q}\right)^{\mathrm{T}}\boldsymbol{P}\left(\frac{1}{2\mu}\boldsymbol{P}^{-1}\boldsymbol{\varepsilon} - \frac{1}{2}\boldsymbol{P}^{-1}\boldsymbol{Q}\right) + \left(\frac{1}{2\mu}\boldsymbol{P}^{-1}\boldsymbol{\varepsilon} - \frac{1}{2}\boldsymbol{P}^{-1}\boldsymbol{Q}\right)^{\mathrm{T}}\boldsymbol{Q} \\ &= \frac{1}{4\mu^2}\boldsymbol{\varepsilon}^{\mathrm{T}}\boldsymbol{P}^{-1}\boldsymbol{\varepsilon} - \frac{1}{4}\boldsymbol{Q}^{\mathrm{T}}\boldsymbol{P}^{-1}\boldsymbol{Q} \end{aligned} \tag{14}$$

In the light of Eqs. (1) and (14), the following equation can be found for a point at the yield surface:

$$\frac{1}{4\mu^2}\boldsymbol{\varepsilon}^{\mathrm{T}}\boldsymbol{P}^{-1}\boldsymbol{\varepsilon}-\frac{1}{4}\boldsymbol{Q}^{\mathrm{T}}\boldsymbol{P}^{-1}\boldsymbol{Q}=1 \tag{15}$$

Considering μ is a non-negative plastic proportionality factor, it can be calculated as the following formulation

$$\mu=\sqrt{\frac{\boldsymbol{\varepsilon}^{\mathrm{T}}\boldsymbol{P}^{-1}\boldsymbol{\varepsilon}}{4+\boldsymbol{Q}^{\mathrm{T}}\boldsymbol{P}^{-1}\boldsymbol{Q}}} \tag{16}$$

Meanwhile, based on Eq. (13), the plastic dissipation power for the general criterion (1) can be re-expressed as follows:

$$D(\varepsilon_{ij})=\boldsymbol{\sigma}_{ij}\varepsilon_{ij}=\boldsymbol{\sigma}^{\mathrm{T}}\boldsymbol{\varepsilon}=\left(\frac{1}{2\mu}\boldsymbol{P}^{-1}\boldsymbol{\varepsilon}-\frac{1}{2}\boldsymbol{P}^{-1}\boldsymbol{Q}\right)^{\mathrm{T}}\boldsymbol{\varepsilon}=\frac{1}{2\mu}\boldsymbol{\varepsilon}^{\mathrm{T}}\boldsymbol{P}^{-1}\boldsymbol{\varepsilon}-\frac{1}{2}\boldsymbol{\varepsilon}^{\mathrm{T}}\boldsymbol{P}^{-1}\boldsymbol{Q} \tag{17}$$

According to Eq. (16), the above formulation can be written as

$$D(\varepsilon_{ij})=\frac{1}{2\mu}\boldsymbol{\varepsilon}^{\mathrm{T}}\boldsymbol{P}^{-1}\boldsymbol{\varepsilon}-\frac{1}{2}\boldsymbol{\varepsilon}^{\mathrm{T}}\boldsymbol{P}^{-1}\boldsymbol{Q}=\frac{1}{2}\sqrt{(\boldsymbol{\varepsilon}^{\mathrm{T}}\boldsymbol{P}^{-1}\boldsymbol{\varepsilon})\cdot(4+\boldsymbol{Q}^{\mathrm{T}}\boldsymbol{P}^{-1}\boldsymbol{Q})}-\frac{1}{2}\boldsymbol{\varepsilon}^{\mathrm{T}}\boldsymbol{P}^{-1}\boldsymbol{Q} \tag{18}$$

Then, the plastic dissipation power is expressed in terms of plastic strain rates. Once the kinematically admissible velocity is obtained, the plastic dissipation power can also be calculated. Therefore, it is not necessary to calculate the stress vector in order to determine the plastic dissipation power. Moreover, the yield surface is not discretized and this reduces the number of constraints significantly for the kinematic limit analysis.

2.4. The nonlinear programming problem

Based on the above analyses, the kinematic limit analysis for frictional materials can be formulated as the following mathematical programming problem:

$$\begin{cases}\lambda=\min\limits_{\boldsymbol{\varepsilon}}\ \int_V\left[\frac{1}{2}\sqrt{(\boldsymbol{\varepsilon}^{\mathrm{T}}\boldsymbol{P}^{-1}\boldsymbol{\varepsilon})\cdot(4+\boldsymbol{Q}^{\mathrm{T}}\boldsymbol{P}^{-1}\boldsymbol{Q})}-\frac{1}{2}\boldsymbol{\varepsilon}^{\mathrm{T}}\boldsymbol{P}^{-1}\boldsymbol{Q}\right]\mathrm{d}v\\ \text{s.t.}\quad \int_{\Gamma_\sigma}\boldsymbol{T}^{\mathrm{T}}\boldsymbol{u}\,\mathrm{d}\Gamma=1\\ \qquad \boldsymbol{\varepsilon}=\frac{1}{2}(\nabla\boldsymbol{u}+\boldsymbol{u}\nabla)\quad \text{in } V\\ \qquad \boldsymbol{u}=\boldsymbol{0}\quad \text{on } \Gamma_u\end{cases} \tag{19}$$

where $\boldsymbol{T}$ is the basic load column vector of surface tractions and $\boldsymbol{u}$ is the displacement column vector.

3. Finite element modelling

The displacement-based finite element method is used in this paper to perform the numerical calculation for the kinematic limit analysis. The structure is first discretized into finite elements $V=\bigcup_{e=1}^{N}V_e$. Then, the displacement velocity and strain rate fields can be interpolated in terms of an unknown nodal displacement velocity vector:

$$\boldsymbol{u}_e(\boldsymbol{x})=\boldsymbol{N}_e(\boldsymbol{x})\boldsymbol{\delta}_e \tag{20}$$

$$\boldsymbol{\varepsilon}_e(\boldsymbol{x})=\boldsymbol{B}_e(\boldsymbol{x})\boldsymbol{\delta}_e \tag{21}$$

where, with reference to the e-th finite element, $\boldsymbol{\delta}_e$ is the nodal displacement velocity column vector, $\boldsymbol{\varepsilon}_e$ is the strain rate column vector, $\boldsymbol{N}_e(\boldsymbol{x})$ is the shape function and $\boldsymbol{B}_e(\boldsymbol{x})$ is the strain function.

$$\boldsymbol{B}_e = [\boldsymbol{B}_1, \boldsymbol{B}_2, \ldots, \boldsymbol{B}_n] \tag{22}$$

where

$$\boldsymbol{B}_i = \begin{bmatrix} \frac{\partial N_i}{\partial x} & 0 & 0 \\ 0 & \frac{\partial N_i}{\partial y} & 0 \\ 0 & 0 & \frac{\partial N_i}{\partial z} \\ \frac{\partial N_i}{\partial y} & \frac{\partial N_i}{\partial x} & 0 \\ 0 & \frac{\partial N_i}{\partial z} & \frac{\partial N_i}{\partial y} \\ \frac{\partial N_i}{\partial z} & 0 & \frac{\partial N_i}{\partial x} \end{bmatrix} \quad (i = 1, 2, \ldots, n) \tag{23}$$

where n is the nodal number of the finite element.

By using the Gaussian integration technique, the objective function in Eq. (19) can be expressed in terms of the nodal displacement velocity as

$$\begin{aligned} &\int_V \left[\frac{1}{2}\sqrt{(\boldsymbol{\varepsilon}^{\mathrm{T}}\boldsymbol{P}^{-1}\boldsymbol{\varepsilon})\cdot(4+\boldsymbol{Q}^{\mathrm{T}}\boldsymbol{P}^{-1}\boldsymbol{Q})} - \frac{1}{2}\boldsymbol{\varepsilon}^{\mathrm{T}}\boldsymbol{P}^{-1}\boldsymbol{Q}\right]\mathrm{d}v \\ &= \sum_{e=1}^{N}\int_{V_e}\left[\frac{1}{2}\sqrt{((\boldsymbol{B}_e\boldsymbol{\delta}_e)^{\mathrm{T}}\boldsymbol{P}^{-1}(\boldsymbol{B}_e\boldsymbol{\delta}_e))\cdot(4+\boldsymbol{Q}^{\mathrm{T}}\boldsymbol{P}^{-1}\boldsymbol{Q})} - \frac{1}{2}((\boldsymbol{B}_e\boldsymbol{\delta}_e)^{\mathrm{T}}\boldsymbol{P}^{-1}\boldsymbol{Q})\right]\mathrm{d}v \\ &= \sum_{e=1}^{N}\sum_{i=1}^{IG}(\rho_e)_i|J|_i\left[\frac{1}{2}\sqrt{(\boldsymbol{\delta}_e^{\mathrm{T}}(\boldsymbol{B}_e^{\mathrm{T}})_i\boldsymbol{P}^{-1}(\boldsymbol{B}_e)_i\boldsymbol{\delta}_e)\cdot(4+\boldsymbol{Q}^{\mathrm{T}}\boldsymbol{P}^{-1}\boldsymbol{Q})} - \frac{1}{2}(\boldsymbol{\delta}_e^{\mathrm{T}}(\boldsymbol{B}_e^{\mathrm{T}})_i\boldsymbol{P}^{-1}\boldsymbol{Q})\right] \\ &= \sum_{e=1}^{N}\sum_{i=1}^{IG}(\rho_e)_i|J|_i\left[\frac{1}{2}\sqrt{(\boldsymbol{\delta}_e^{\mathrm{T}}(\boldsymbol{K}_e)_i\boldsymbol{\delta}_e)\cdot(4+\boldsymbol{Q}^{\mathrm{T}}\boldsymbol{P}^{-1}\boldsymbol{Q})} - \frac{1}{2}(\boldsymbol{\delta}_e^{\mathrm{T}}(\boldsymbol{G}_e)_i)\right] \end{aligned} \tag{24}$$

where $(\rho_e)_i$ is the Gaussian integral weight at the i-th Gaussian integral point in element e, $|J|_i$ is the determinant of the Jacobian matrix at the i-th Gaussian integral point and IG is the number of Gaussian integral points in the finite element e.

$$\boldsymbol{K}_e = \boldsymbol{B}_e^{\mathrm{T}}\boldsymbol{P}^{-1}\boldsymbol{B}_e \tag{25}$$

$$\boldsymbol{G}_e = \boldsymbol{B}_e^{\mathrm{T}}\boldsymbol{P}^{-1}\boldsymbol{Q} \tag{26}$$

By introducing the transformation matrix of each element $\boldsymbol{C}_e$, the nodal displacement velocity vector $\boldsymbol{\delta}_e$ for each element can be expressed by the global nodal displacement velocity vector $\boldsymbol{\delta}$ for the structure.

$$\boldsymbol{\delta}_e = \boldsymbol{C}_e\cdot\boldsymbol{\delta} \tag{27}$$

Then, Eq. (24) can be recast as

$$\begin{aligned} &\int_V \left[\frac{1}{2}\sqrt{(\boldsymbol{\varepsilon}^{\mathrm{T}}\boldsymbol{P}^{-1}\boldsymbol{\varepsilon})\cdot(4+\boldsymbol{Q}^{\mathrm{T}}\boldsymbol{P}^{-1}\boldsymbol{Q})} - \frac{1}{2}\boldsymbol{\varepsilon}^{\mathrm{T}}\boldsymbol{P}^{-1}\boldsymbol{Q}\right]\mathrm{d}v \\ &= \sum_{e=1}^{N}\sum_{i=1}^{IG}(\rho_e)_i|J|_i\left[\frac{1}{2}\sqrt{(\boldsymbol{\delta}_e^{\mathrm{T}}(\boldsymbol{K}_e)_i\boldsymbol{\delta}_e)\cdot(4+\boldsymbol{Q}^{\mathrm{T}}\boldsymbol{P}^{-1}\boldsymbol{Q})} - \frac{1}{2}(\boldsymbol{\delta}_e^{\mathrm{T}}(\boldsymbol{G}_e)_i)\right] \\ &= \sum_{i\in I}\rho_i|J|_i\left[\frac{1}{2}\sqrt{(\boldsymbol{\delta}^{\mathrm{T}}\boldsymbol{K}_i\boldsymbol{\delta})\cdot(4+\boldsymbol{Q}^{\mathrm{T}}\boldsymbol{P}^{-1}\boldsymbol{Q})} - \frac{1}{2}(\boldsymbol{\delta}^{\mathrm{T}}\boldsymbol{G}_i)\right] \end{aligned} \tag{28}$$

where I denotes the set of all Gaussian integral points of the FE discretized structure, and

$$\boldsymbol{K}_i = \boldsymbol{C}_e^{\mathrm{T}}(\boldsymbol{K}_e)_i \boldsymbol{C}_e \tag{29}$$

$$\boldsymbol{G}_i = \boldsymbol{C}_e^{\mathrm{T}}(\boldsymbol{G}_e)_i \tag{30}$$

After the discretization, the normalization condition in Eq. (19) can be expressed in terms of the nodal velocity fields as

$$\boldsymbol{F}^{\mathrm{T}}\boldsymbol{\delta} = 1 \tag{31}$$

where $\boldsymbol{F}$ is the basic column vector of equivalent nodal loads.

Finally, the finite element modelling of kinematic limit analysis for the frictional materials can be expressed as the following minimum optimization problem

$$\lambda = \min_{\boldsymbol{\delta}} \sum_{i\in I} \rho_i |J|_i \left[\frac{1}{2}\sqrt{(\boldsymbol{\delta}^{\mathrm{T}}\boldsymbol{K}_i\boldsymbol{\delta})\cdot(4+\boldsymbol{Q}^{\mathrm{T}}\boldsymbol{P}^{-1}\boldsymbol{Q})} - \frac{1}{2}(\boldsymbol{\delta}^{\mathrm{T}}\boldsymbol{G}_i)\right] \tag{32a}$$

$$\text{s.t.} \quad \boldsymbol{F}^{\boldsymbol{T}}\boldsymbol{\delta} = 1 \tag{32b}$$

After the displacement boundary condition is imposed by means of the conventional finite element technique, a minimum optimized upper bound λ to the plastic limit load multiplier of the structure can be obtained by solving the above mathematical programming problem. The plastic limit load of the structure is given by $\lambda\boldsymbol{F}$.

4. The iterative solution algorithm

The kinematic (upper bound) limit analysis defined by Eq. (32) is a minimum optimization problem with a single equality constraint. The objective function is nonlinear, continuous but may be nondifferentiable. For a continuous and differentiable quadratic mathematical programming problem under the Kuhn–Tucker's conditions, several effective methods can be used to solve it (Himmelblau, 1972).

For the mathematical programming problem Eq. (32), there is a calculation of square root which could make the objective function unsmooth and nondifferentiable. This causes some difficulties in solving the programming problem. For a linear nondifferentiable programming problem, if the objective function is finite and continuous in a feasible set, it is not necessary to be differentiable everywhere and an optimal solution can be obtained (Shapiro, 1979). The nonlinear objective function was shown to be nondifferentiable in rigid areas for limit analysis using the von Mises criterion (Zhang et al., 1991; Zhang and Lu, 1995; Liu et al., 1995; Chen et al., 1998; Li et al., 2001, 2003). The difficulty was then overcome by using an iterative algorithm (Zhang et al., 1991), where a technique based on distinguishing rigid/plastic areas was put forward. This technique is similar to the procedure used by Huh and Yang (1991) and will be used in this study to solve the nonlinear mathematical programming problem Eq. (32).

By using the Lagrangean method (Himmelblau, 1972), the equality constraint can be removed from Eq. (32). Then, an unconstrained minimum optimization problem can be obtained as follows:

$$L(\boldsymbol{\delta}, q) = \sum_{i\in I} \rho_i |J|_i \left[\frac{1}{2}\sqrt{(\boldsymbol{\delta}^{\mathrm{T}}\boldsymbol{K}_i\boldsymbol{\delta})\cdot(4+\boldsymbol{Q}^{\mathrm{T}}\boldsymbol{P}^{-1}\boldsymbol{Q})} - \frac{1}{2}(\boldsymbol{\delta}^{\mathrm{T}}\boldsymbol{G}_i)\right] + q(1-\boldsymbol{F}^{\mathrm{T}}\boldsymbol{\delta}) \tag{33}$$

where q is the Lagrangean multiplier.

In order to perform an iteration technique for solving the nonlinear programming problem, Eq. (33) can be re-written as

$$L(\boldsymbol{\delta}, q) = \sum_{i\in I} \rho_i |J|_i \left[\frac{1}{2} \frac{(\boldsymbol{\delta}^{\mathrm{T}} \boldsymbol{K}_i \boldsymbol{\delta}) \cdot (4 + \boldsymbol{Q}^{\mathrm{T}} \boldsymbol{P}^{-1} \boldsymbol{Q})}{\boldsymbol{\omega}^{(ICP)}} - \frac{1}{2} (\boldsymbol{\delta}^{\mathrm{T}} \boldsymbol{G}_i) \right] + q(1 - \boldsymbol{F}^{\mathrm{T}} \boldsymbol{\delta}) \tag{34}$$

where $\boldsymbol{\omega}^{(ICP)} = \sqrt{(\boldsymbol{\delta}^{\mathrm{T}} \boldsymbol{K}_i \boldsymbol{\delta}) \cdot (4 + \boldsymbol{Q}^{\mathrm{T}} \boldsymbol{P}^{-1} \boldsymbol{Q})}$ and the superscript '*ICP*' denotes $\boldsymbol{\omega}$ is an iteration control parameter.

To overcome the difficulties which may arise from an unsmooth objective function (32a), all of nondifferentiable areas need to be identified where the first part of the plastic dissipation power becomes zero (i.e., $\sqrt{(\boldsymbol{\delta}^{\mathrm{T}} \boldsymbol{K}_i \boldsymbol{\delta}) \cdot (4 + \boldsymbol{Q}^{\mathrm{T}} \boldsymbol{P}^{-1} \boldsymbol{Q})} = 0$). In order to find all nondifferentiable regions, an iteration technique is needed. The iteration starts from the hypothesis that the strain rate is non-zero everywhere and the nondifferentiable region does not exist at first iteration step. However, from the second iteration step, the strain rate will be updated and the nondifferentiable region can be identified by checking whether $\sqrt{(\boldsymbol{\delta}^{\mathrm{T}} \boldsymbol{K}_i \boldsymbol{\delta}) \cdot (4 + \boldsymbol{Q}^{\mathrm{T}} \boldsymbol{P}^{-1} \boldsymbol{Q})}$ is equal to zero. All nondifferentiable areas will be found by means of this step-by-step technique.

Once a nondifferentiable region is found at an iteration step, the condition $(\sqrt{(\boldsymbol{\delta}^{\mathrm{T}} \boldsymbol{K}_i \boldsymbol{\delta}) \cdot (4 + \boldsymbol{Q}^{\mathrm{T}} \boldsymbol{P}^{-1} \boldsymbol{Q})} = 0)$ will be introduced as a constraint into the mathematical programming problem by means of the penalty function method. Therefore, the objective function will be modified at each iteration step until the limit load multiplier is determined.

Based on the above analyses, an iterative solution algorithm for calculating the limit load multiplier is proposed as follows:

Step 0: initializing the nonlinear objective function

As shown in Huh and Yang (1991) and Liu et al. (1995), the selection of the initial nodal velocity field does not affect the convergence of iteration. It may be proved that from any initial trial solution, the subsequent iterations are locked in a certain convex hull that contains the exact solution of the problem (Huh and Yang, 1991). For simplicity, we follow Zhang and Lu (1995) and start iteration by defining an iteration seed $(\boldsymbol{\omega}^{(ICP)})_0 = 1$ in Eq. (34). Then, the initial nodal displacement vector $\boldsymbol{\delta}_0$ can be estimated by solving the following mathematical programming problem:

$$L(\boldsymbol{\delta}, q) = \sum_{i\in I} \rho_i |J|_i \left[\frac{1}{2} ((\boldsymbol{\delta}^{\mathrm{T}} \boldsymbol{K}_i \boldsymbol{\delta}) \cdot (4 + \boldsymbol{Q}^{\mathrm{T}} \boldsymbol{P}^{-1} \boldsymbol{Q})) - \frac{1}{2} (\boldsymbol{\delta}^{\mathrm{T}} \boldsymbol{G}_i) \right] + q(1 - \boldsymbol{F}^{\mathrm{T}} \boldsymbol{\delta}) \tag{35}$$

Using the minimum optimization theory, the following system of linear equations can be obtained by applying $\frac{\partial L}{\partial \boldsymbol{\delta}} = \mathbf{0}$ and $\frac{\partial L}{\partial q} = 0$:

$$\begin{cases} \sum_{i\in I} \rho_i |J|_i \left[((\boldsymbol{K}_i \boldsymbol{\delta}) \cdot (4 + \boldsymbol{Q}^{\mathrm{T}} \boldsymbol{P}^{-1} \boldsymbol{Q})) - \frac{1}{2} \boldsymbol{G}_i \right] = q\boldsymbol{F} \\ \mathbf{F}^{\mathbf{T}} \boldsymbol{\delta} = 1 \end{cases} \tag{36}$$

By solving the above system of linear equations (36), we can obtain the initial nodal displacement velocity vector $\boldsymbol{\delta}_0$. Then, the initial load multiplier can be calculated by using

$$\lambda_0 = \sum_{i\in I} \rho_i |J|_i \left[\frac{1}{2} \sqrt{(\boldsymbol{\delta}_0^{\mathrm{T}} \boldsymbol{K}_i \boldsymbol{\delta}_0) \cdot (4 + \boldsymbol{Q}^{\mathrm{T}} \boldsymbol{P}^{-1} \boldsymbol{Q})} - \frac{1}{2} \boldsymbol{\delta}_0^{\mathrm{T}} \boldsymbol{G}_i \right] \tag{37}$$

Step k + 1 (k = 0,1,2, ...): distinguishing the nondifferentiable areas to revise the objective function

Based on the computational results at step k, the value of $\sqrt{(\boldsymbol{\delta}^{\mathrm{T}}\boldsymbol{K}_i\boldsymbol{\delta})\cdot(4+\boldsymbol{Q}^{\mathrm{T}}\boldsymbol{P}^{-1}\boldsymbol{Q})}(i\in I)$ needs to be calculated at every Gaussian integral point of the finite element discretized structure in order to check whether it is in a nondifferentiable area. Then the Gaussian integral point set I will be subdivided into two subsets: the subset $(I_R)_{k+1}$ where the objective function is not differentiable and the subset $(I_P)_{k+1}$ where the objective function is differentiable.

$$I=(I_R)_{k+1}\cup(I_P)_{k+1} \tag{38a}$$

$$(I_R)_{k+1}=\left\{i\in I,\sqrt{(\boldsymbol{\delta}_k^{\mathrm{T}}\boldsymbol{K}_i\boldsymbol{\delta}_k)\cdot(4+\boldsymbol{Q}^{\mathrm{T}}\boldsymbol{P}^{-1}\boldsymbol{Q})}=0\right\} \tag{38b}$$

$$(I_P)_{k+1}=\left\{i\in I,\sqrt{(\boldsymbol{\delta}_k^{\mathrm{T}}\boldsymbol{K}_i\boldsymbol{\delta}_k)\cdot(4+\boldsymbol{Q}^{\mathrm{T}}\boldsymbol{P}^{-1}\boldsymbol{Q})}\neq 0\right\} \tag{38c}$$

However, considering that there is a limitation of storage for a computer and that any attempt to evaluate the gradient of a square root near a zero argument would cause computational overflow, a small real number $\zeta(\zeta\to 0)$ is needed in a computer program to distinguish the differentiable and nondifferentiable regions. In other words, a region with $\sqrt{(\boldsymbol{\delta}^{\mathrm{T}}\boldsymbol{K}_i\boldsymbol{\delta})\cdot(4+\boldsymbol{Q}^{\mathrm{T}}\boldsymbol{P}^{-1}\boldsymbol{Q})}<\zeta$ can be regarded as nondifferentiable. From a theoretical point of view, the smaller ζ is, the more precise the numerical calculation would be. In practice, however, the value ζ adopted in a computer program may vary from 10^{-8} to 10^{-12}. The numerical calculations suggest that when ζ is less than 10^{-8}, it has very little effect on the results. A similar smoothing parameter was also adopted by Huh and Yang (1991) to remove the same numerical difficulty in their limit analysis formulation.

The value of $\boldsymbol{\delta}_k$ at this iterative step can then be determined by solving the following mathematical programming problem

$$\begin{cases}\min\limits_{\boldsymbol{\delta}} \sum\limits_{i\in(I_P)_{k+1}}\rho_i|J|_i\left[\frac{1}{2}\frac{(\boldsymbol{\delta}^{\mathrm{T}}\boldsymbol{K}_i\boldsymbol{\delta})\cdot(4+\boldsymbol{Q}^{\mathrm{T}}\boldsymbol{P}^{-1}\boldsymbol{Q})}{\sqrt{(\boldsymbol{\delta}_k^{\mathrm{T}}\boldsymbol{K}_i\boldsymbol{\delta}_k)\cdot(4+\boldsymbol{Q}^{\mathrm{T}}\boldsymbol{P}^{-1}\boldsymbol{Q})}}-\frac{1}{2}\boldsymbol{\delta}^{\mathrm{T}}\boldsymbol{G}_i\right]\\ \text{s.t.}\quad \boldsymbol{F}^{\mathrm{T}}\boldsymbol{\delta}=1\\ \qquad (\boldsymbol{\delta}^{\mathrm{T}}\boldsymbol{K}_i\boldsymbol{\delta})\cdot(4+\boldsymbol{Q}^{\mathrm{T}}\boldsymbol{P}^{-1}\boldsymbol{Q})=0\quad (i\in(I_R)_{k+1})\end{cases} \tag{39}$$

which is equivalent to the following minimum optimization problem:

$$\begin{aligned}L(\boldsymbol{\delta},q)=&\sum_{i\in(I_P)_{k+1}}\rho_i|J|_i\left[\frac{1}{2}\frac{(\boldsymbol{\delta}^{\mathrm{T}}\boldsymbol{K}_i\boldsymbol{\delta})\cdot(4+\boldsymbol{Q}^{\mathrm{T}}\boldsymbol{P}^{-1}\boldsymbol{Q})}{\sqrt{(\boldsymbol{\delta}_k^{\mathrm{T}}\boldsymbol{K}_i\boldsymbol{\delta}_k)\cdot(4+\boldsymbol{Q}^{\mathrm{T}}\boldsymbol{P}^{-1}\boldsymbol{Q})}}-\frac{1}{2}\boldsymbol{\delta}^{\mathrm{T}}\boldsymbol{G}_i\right]\\ &+\alpha\sum_{i\in(I_R)_{k+1}}\rho_i|J|_i[((\boldsymbol{\delta}^{\mathrm{T}}\boldsymbol{K}_i\boldsymbol{\delta})\cdot(4+\boldsymbol{Q}^{\mathrm{T}}\boldsymbol{P}^{-1}\boldsymbol{Q}))]+q(1-\boldsymbol{F}^{\mathrm{T}}\boldsymbol{\delta})\end{aligned} \tag{40}$$

where α is a penalty factor and its value may vary from 10^6 to 10^{12}.

Finally, the minimum optimization problem (40) can be transformed into the following system of linear algebraic equations by applying $\frac{\partial L}{\partial\boldsymbol{\delta}}=\boldsymbol{0}$ and $\frac{\partial L}{\partial q}=0$

$$\begin{cases}\sum\limits_{i\in(I_P)_{k+1}}\rho_i|J|_i\left[\frac{(\boldsymbol{K}_i\boldsymbol{\delta})\cdot(4+\boldsymbol{Q}^{\mathrm{T}}\boldsymbol{P}^{-1}\boldsymbol{Q})}{\sqrt{(\boldsymbol{\delta}_k^{\mathrm{T}}\boldsymbol{K}_i\boldsymbol{\delta}_k)\cdot(4+\boldsymbol{Q}^{\mathrm{T}}\boldsymbol{P}^{-1}\boldsymbol{Q})}}-\frac{1}{2}\boldsymbol{G}_i\right]\\ +2\alpha\sum\limits_{i\in(I_R)_{k+1}}\rho_i|J|_i[(\boldsymbol{K}_i\boldsymbol{\delta})\cdot(4+\boldsymbol{Q}^{\mathrm{T}}\boldsymbol{P}^{-1}\boldsymbol{Q})]=q\boldsymbol{F}\\ \boldsymbol{F}^{\mathrm{T}}\boldsymbol{\delta}=1\end{cases} \tag{41}$$

By solving the above system of linear equations defined in Eq. (41), we can obtain the nodal displacement velocity vector $\boldsymbol{\delta}_{k+1}$ at this step. The limit load multiplier at this step can then be calculated as

$$\lambda_{k+1} = \sum_{i\in I} \rho_i |J|_i \left[\frac{1}{2} \sqrt{(\boldsymbol{\delta}_{k+1}^{\mathrm{T}} \boldsymbol{K}_i \boldsymbol{\delta}_{k+1}) \cdot (4 + \boldsymbol{Q}^{\mathrm{T}} \boldsymbol{P}^{-1} \boldsymbol{Q})} - \frac{1}{2} \boldsymbol{\delta}_{k+1}^{\mathrm{T}} \boldsymbol{G}_i \right] \tag{42}$$

The above iterative process is repeated until the following convergence criteria are satisfied

$$\begin{cases} \dfrac{|\lambda_{k+1} - \lambda_k|}{\lambda_{k+1}} \leqslant \eta_1 \\ \dfrac{\|\boldsymbol{\delta}_{k+1} - \boldsymbol{\delta}_k\|}{\|\boldsymbol{\delta}_{k+1}\|} \leqslant \eta_2 \end{cases} \tag{43}$$

where η_1 and η_2 are computational error tolerances.

The above procedure leads to the limit load multiplier λ through a convergent sequence with monotonically decreasing series λ_k and a minimum optimum upper bound to the limit load multiplier may be obtained.

The solution algorithm proposed in this paper for frictional materials has been based on the technique originally developed by Zhang et al. (1991) for von Mises' criterion for which convergence has been proved. It is stressed that similar procedures have also been successfully used by many other researchers (Huh and Yang, 1991; Liu et al., 1995; Zhang and Lu, 1995; Maier et al., 2000). Although all the numerical results presented in this study show clearly that the procedure is very stable and convergent, further theoretical study of the effect of a general nonlinear yield criterion on the performance of the proposed iterative procedure may be useful.

5. Applications

The proposed numerical method described in this paper is now applied to evaluate the stability problems of some typical soil structures. The efficiency of the developed nonlinear kinematic algorithm for the frictional yield criterion in the form (1) has also been proved. In this section, for the plane strain model, the Mohr–Coulomb criterion is used to describe the yield of a frictional material while for the plane stress model, the Drucker–Prager yield surface is adopted. In the plane stress model, the strength parameters φ_0 and c_0 in the Drucker–Prager criterion is determined by:

$$\varphi_0 = \frac{1}{2\sqrt{3}} \sin\varphi \tag{44}$$

$$c_0 = \frac{2}{\sqrt{3}} \cos\varphi \cdot c \tag{45}$$

5.1. A half-space under normal pressure

The first numerical example to be illustrated is the stability problem of an isotropic and homogeneous half-space under a uniform normal pressure, as shown in Fig. 1. A weightless cohesive-frictional soil material is considered and the Mohr–Coulomb criterion is used to model its plastic behavior. The plane strain condition is assumed. The exact collapse pressure for this problem is given by Prandtl (1920) as:

$$\begin{cases} p_{\mathrm{s}} = c \cdot \cot\varphi \cdot \left[\tan^2\left(\frac{\pi}{4} + \frac{\varphi}{2}\right) \cdot e^{\pi \cdot \tan\varphi} - 1 \right] & (\varphi > 0^\circ) \\ p_{\mathrm{s}} = 5.14c \quad (\varphi = 0^\circ) \end{cases} \tag{46}$$

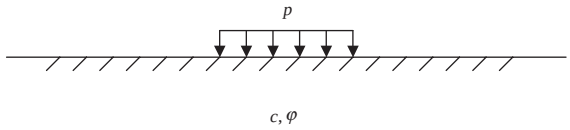

Fig. 1. A half-space under uniform normal pressure.

where p_s denotes the plastic limit load of the half-space under a uniform normal pressure, c and φ are the effective cohesion and the effective friction angle of the soil material respectively.

To simulate a half-space, a finite region is determined to be numerically calculated by means of the proposed method. The size of the selected finite region must be sufficiently large so that a half-space requirement is approximately satisfied. This is mainly dependent on the area of the contact loading. Due to the symmetry of the geometry and loading, only half of the body is analyzed. In this plane strain example, the size of the simulated region required is determined as: $L_0/B_0 = 16$ and $H_0/B_0 = 4$, where B_0 denotes the length of loading area, L_0 and H_0 denote the length and height of the simulated region respectively. The selected body is discretized with 2400 eight-node quadrilateral finite elements as shown in Fig. 2 and the convergence tolerances are $\eta_1 = \eta_2 = 10^{-3}$. The numerical results are shown in Fig. 3 and they are in good agreement with the Prandtl's exact solution (1920).

The relationship between the iterative convergence sequences $\lambda_k(\lambda = p_s/c)$ and the iterative step k with various internal friction angles φ is shown in Fig. 4. The results show that the efficiency and numerical stability of the proposed algorithm are fairly high and that the amount of computational effort is very small. It can be concluded from the numerical results that the internal friction angle of the soil material has a significant effect on the bearing-capacity and stability of the half-space under normal pressure.

To further show the failure mechanism of the half-space, some typical failure modes are plotted in Figs. 5–8. It can be seen that for the half-space under normal pressure, the body will collapse when the plastic

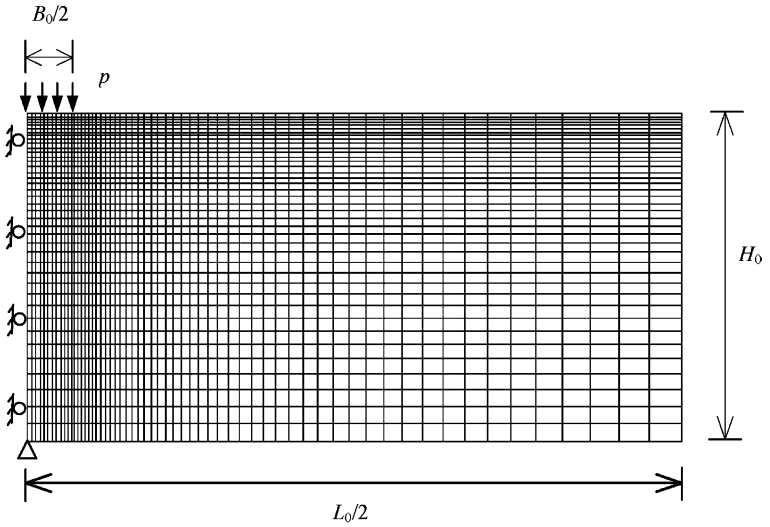

Fig. 2. The finite element mesh of the half-space.

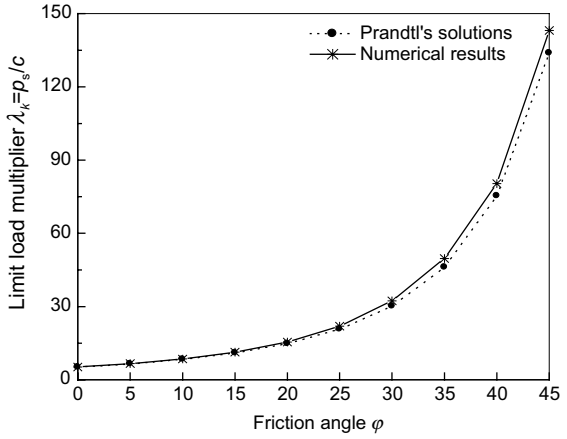

Fig. 3. The limit loads of the half-space under uniform pressure.

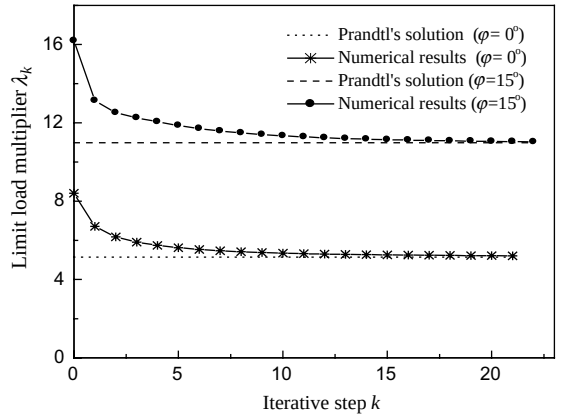

Fig. 4. The convergence sequence $\lambda_k(p_s/c)$ with iterative steps.

Fig. 5. The plastic velocity of the half-space ($\varphi = 0°$).

zone is large enough for plastic sliding to occur. When the plastic zone starts to penetrate through the whole structure, the non-restricted plastic flow will occur and the structure will fail.

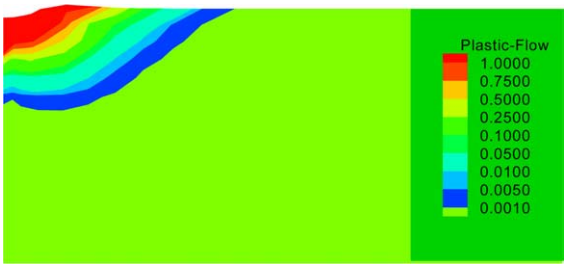

Fig. 6. The plastic dissipation factor of the half-space ($\varphi = 0°$).

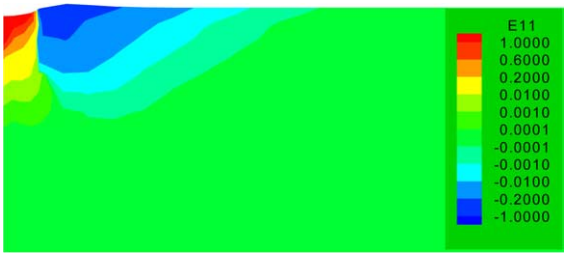

Fig. 7. The plastic velocity of the half-space ($\varphi = 15°$).

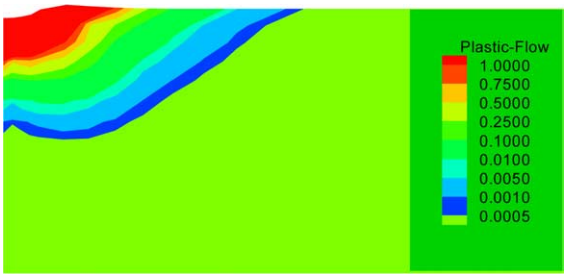

Fig. 8. The plastic dissipation factor of the half-space ($\varphi = 15°$).

5.2. Thick-walled cylinder under internal pressure

Components in engineering structures such as pipes can be simplified as a thick-walled cylinder problem. Now consider a long thick-walled cylinder with inner radius R_1 and outer radius R_2 subject to a uniform internal pressure p. Under the conditions of plane strain and the Mohr–Coulomb criterion, the exact solution to the plastic limit load of this case has been obtained by Yu (1992) and can be given by the following equation:

$$p_s = \frac{Y + (\alpha - 1)p_0}{(\alpha - 1)} \left(\left(\frac{R_2}{R_1} \right)^{(\alpha-1)/\alpha} - 1 \right) + p_0 \tag{47}$$

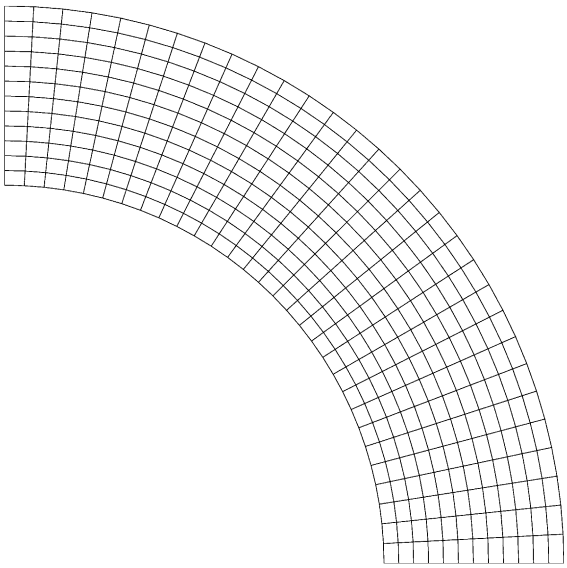

Fig. 9. The finite element mesh of the cylinder.

where p_s denotes the collapse pressure, p_0 is the initial hydrostatic pressure acting throughout the structure, Y and α are material constants determined by

$$Y = \frac{2c\cos\varphi}{1-\sin\varphi} \tag{48}$$

$$\alpha = \tan^2(45^\circ + \varphi/2) \tag{49}$$

where c and φ are the cohesion and internal friction angle of a cohesive-frictional material respectively.

Because of symmetry, only a quarter of the structure is discretized for the FE analysis and one of the meshes used for the numerical calculation is shown in Fig. 9. The numerical results of the bearing capacities of the cylinder are calculated, as shown in Fig. 10, where the initial hydrostatic pressure is not considered, i.e. $p_0 = 0$, and the Mohr–Coulomb criterion is used. There is a good agreement between the numerical results by the proposed method and the analytical solutions from Eq. (47).

The numerical results for three different meshes are provided in Table 1 to further demonstrate the efficiency of the proposed nonlinear algorithm for the kinematic limit analysis based on the Mohr–Coulomb criterion. The simulation is performed for the case with $R_2/R_1 = 1.5$, $\varphi = 30^\circ$ and $\eta_1 = \eta_2 = 10^{-3}$ on a PC machine with a Pentium IV 3.2GH CPU and 2.0GB RAM under Windows XP. The complier used is Compaq Visual Fortran Professional Edition 6.5.0. It can be seen that for a predetermined problem, the number of iterations is independent of the mesh density. This can be also concluded from the last example. Using the proposed algorithm, the convergence solutions can be obtained only after a few iterations and only a little CPU time is spent. The results also show that the nonlinear technique has the advantages of high computational precision and good numerical stability.

5.3. Stability of a bridge under a force

The stability of a bridge under a concentrated force is another important engineering problem. In this section, a simple structural design for the bridge is provided, as shown in Fig. 11. The plane stress model

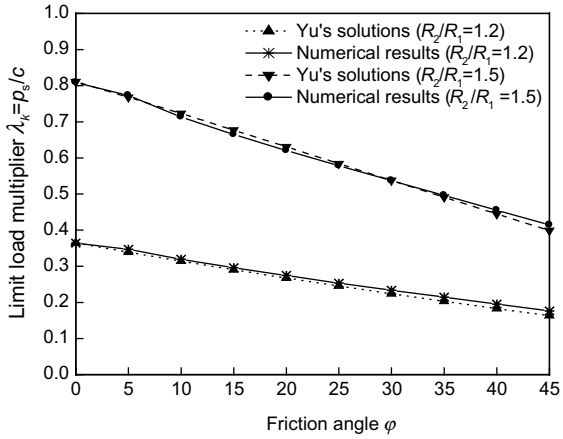

Fig. 10. The plastic limit loads of the cylinder under internal pressure.

Table 1
Effect of different meshes on the performance of kinematic limit analysis

Mesh	Number of iterations	CPU time (s)	Limit load p_s/c	Percentage error (%)
Coarse, 180 elements, 597 nodes	24	28	0.5373	0.06
Medium, 360 elements, 1165 nodes	24	56	0.5375	0.02
Fine, 600 elements, 1901 nodes	24	92	0.5376	0.0

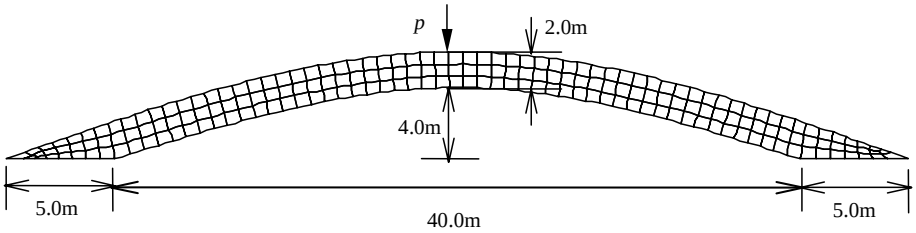

Fig. 11. The finite element mesh of the bridge.

is assumed and the Drucker–Prager criterion is adopted. The bridge is discretized with 190 eight-node quadrilateral finite elements and the convergence tolerances are determined as $\eta_1 = \eta_2 = 10^{-3}$. The bearing capacities of the bridge with $\varphi = 5°$ are calculated and shown in Fig. 12, where L_0 denotes the distance from the point of loading to the central point of the bridge. It can be seen that the most dangerous loading point is located at the center of the bridge. More detailed failure modes of the bridge are shown in Figs. 13–16. From these results, it can be concluded that the collapse of the structure is due to the development of plastic zones penetrating through the structure. For a bridge under a concentrated force, the bearing capacity is dependent on its thickness and also influenced by its supports. Even if the loading is applied at the center of the bridge, far away from the supports, there are still some plastic zones near the supports at the collapse of the structure.

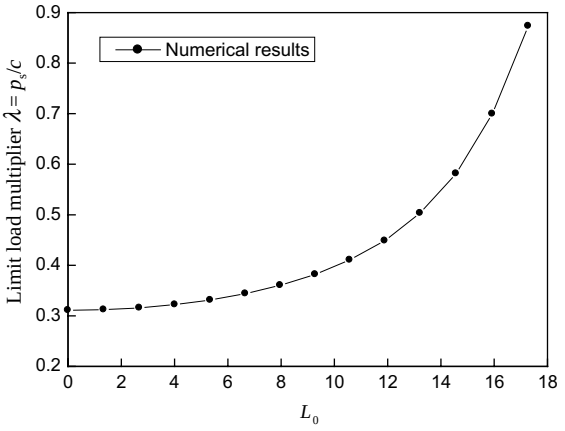

Fig. 12. The limit loads of the bridge under a force.

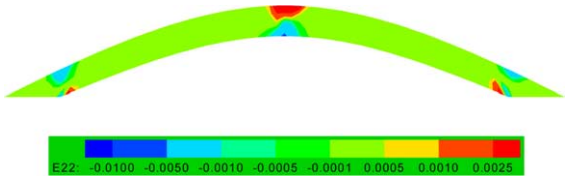

Fig. 13. The plastic velocity of the bridge ($L_0 = 0.0$ m).

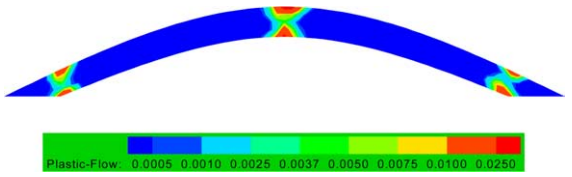

Fig. 14. The plastic dissipation factor of the bridge ($L_0 = 0.0$ m).

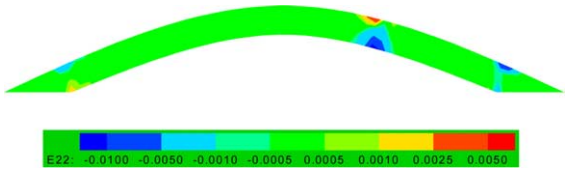

Fig. 15. The plastic velocity of the bridge ($L_0 = 9.28$ m).

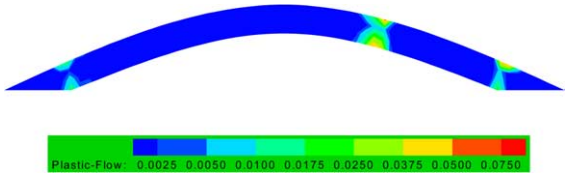

Fig. 16. The plastic dissipation factor of the bridge ($L_0 = 9.28$ m).

6. Conclusions

A novel iterative procedure has been developed to conduct kinematic limit analysis for frictional materials and its numerical implementation is performed by means of a nonlinear programming technique in conjunction with the displacement-based finite element method. The method proposed in the paper is an extension of the nonlinear programming technique that has so far only been applied to non-frictional materials such as those governed by von Mises' or Hill's yield criteria (Zhang et al., 1991; Zhang and Lu, 1995; Liu et al., 1995). By using an associated flow rule, a general pressure-sensitive yield criterion can be directly introduced into the kinematic theorem of limit analysis. A nonlinear function of the kinematically admissible velocity field is then obtained to represent the plastic dissipation power. The yield surface does not need to be linearized which can reduce the number of constraints and therefore computational costs. Based on the mathematical programming theory, a finite element formulation of the kinematic limit analysis procedure is proposed as a nonlinear programming problem subject to a single equality constraint. The proposed method only makes use of the kinematically admissible velocity field and no stress fields need to be calculated for performing limit analysis. The numerical examples show that the proposed iterative algorithm has the advantages of high computational accuracy and good numerical stability. By means of the proposed method, possible failure mechanisms of a structure can also be obtained.

Acknowledgements

The research reported in this paper is supported by a grant from the UK's Engineering and Physical Sciences Research Council (EPSRC) and the authors are grateful for this support. The authors also wish to thank one of the referees for his/her constructive comments that have led to improvements on the clarity of the paper.

References

Capsoni, A., Corradi, L., Vena, P., 2001. Limit analysis of orthotropic structures based on Hill's yield condition. Int. J. Solids & Structures 38, 3945–3963.

Chen, H.F., Liu, Y.H., Cen, Z.Z., Xu, B.Y., 1998. Numerical analysis of limit load and reference stress of defective pipelines under multi-loading systems. Int. J. Pressure Vessels Piping 75, 105–114.

Chen, W.F., 1975. Limit Analysis and Soil Plasticity. Elsevier, Amsterdam.

Drucker, D.C., 1953. Limit analysis of two and three-dimensional soil mechanics problems. J. Mech. Phys. Solids 1, 217–226.

Francescato, P., Pastor, J., 1997. Lower and upper numerical bounds to the off-axis strength of unidirectional fiber-reinforced composite by limit analysis methods. Eur. J. Mech. A/Solids 16, 213–234.

Himmelblau, D.M., 1972. Applied Nonlinear Programming. McGraw-Hill Book Company, New York.

Huh, H., Yang, W.H., 1991. A general algorithm for limit solutions of plane stress problems. Int. J. Solids Struct. 28, 727–738.

Li, H.X., Liu, Y.H., Feng, X.Q., Cen, Z.Z., 2001. Micro/macromechanical plastic limit analyses of composite materials and structures. Acta Mechanica Solida Sinica 14, 323–333.

Li, H.X., Liu, Y.H., Feng, X.Q., Cen, Z.Z., 2003. Limit analysis of ductile composites based on homogenization theory. Proc. R. Soc. London, Ser. A 459, 659–675.

Liu, Y.H., Cen, Z.Z., Xu, B.Y., 1995. A numerical method for plastic limit analysis of 3-D structures. Int. J. Solids Struct. 32, 1645–1658.

Lyamin, A.V., Sloan, S.W., 2002a. Upper bound limit analysis using linear finite elements and non-linear programming. Int. J. Numer. Anal. Meth. Geomech. 26, 181–216.

Lyamin, A.V., Sloan, S.W., 2002b. Lower bound limit analysis using non-linear programming. Int. J. Numer. Meth. Engng. 55, 573–611.

Lysmer, J., 1970. Limit analysis of plane problems in soil mechanics. J. Soil. Mech. Found. Div., ASCE 96, 1311–1334.

Maier, G., 1969. Shakedown theory in perfect elastoplasticity with associated and nonassociated flow-laws: a finite element linear programming approach. Meccanica 4, 250–260.

Maier, G, Carvelli, G., Cocchetti, G, 2000. On direct methods of shakedown and limit analysis. Plenary Lecture, 4th Euromech Solid Mechanics Conference, Metz, June 2000.

Ponter, A.R.S., Carter, K.F., 1997. Limit state solutions based upon linear elastic solutions with a spatially varying elastic modulus. Comp. Meth. Appl. Mech. Engng. 140, 237–258.

Ponter, A.R.S., Fuschi, P., Engelhardt, M., 2000. Limit analysis for a general class of yield conditions. Eur. J. Mech. A/Solids 19, 401–421.

Ponter, A.R.S., Chen, H.F., Boulbibane, M., Habibullah, M., 2002. The linear matching method for the evaluation of limit loads, shakedown limits and related problems. In: Fifth World Congress on Computational Mechanics, Austria.

Prandtl, L., 1920. Über die Härte plastischer Körper. Nachrichten von der Gesellschaft der Wissenschaften zu Göttingen, Mathematisch- Physikalische Klasse 12, 74–85.

Shapiro, J.F., 1979. Mathematical Programming: Structures and Algorithms. A Wiley-Interscience Publication, New York.

Sloan, S.W., 1988. Lower bound limit analysis using finite elements and linear programming. Int. J. Numerical Anal. Methods Geomechanics 12, 2671–2685.

Sloan, S.W., Kleeman, P.W., 1995. Upper bound limit analysis using discontinuous velocity fields. Comp. Methods Appl. Mech. Engng. 127, 293–314.

Turgeman, S., Pastor, J., 1982. Limit analysis: a linear formulation of the kinematic approach for axisymmetric mechanic problems. Int. J. Num. Anal. Meth. Geomech. 6, 109–128.

Yu, H.S., 1992. Expansion of a thick cylinder of soils. Comp. Geotech. 14, 21–41.

Yu, H.S., Sloan, S.W., 1994. Limit analysis of anisotropic soils using finite elements and linear programming. Mech. Res. Commun. 6, 545–554.

Yu, H.S., Sloan, S.W., Kleeman, P.W., 1994. A quadratic element for upper bound limit analysis. Engng. Comput. 11, 195–212.

Yu, H.S., Sloan, S.W., 1997. Finite element limit analysis of reinforced soils. Comput. Struct. 3, 567–577.

Zhang, P.X., Lu, M.W., Hwang, K., 1991. A mathematical programming algorithm for limit analysis. Acta Mech. Sinica 7, 267–274 (in English).

Zhang, Y.G., Lu, M.W., 1995. An algorithm for plastic limit analysis. Comp. Meth. Appl. Mech. Engrg. 126, 333–341.

Zouain, N., Herskovits, J., Borges, L.A., Feijóo, R.A., 1993. An iterative algorithm for limit analysis with nonlinear yield functions. Int. J. Solids Struct. 30, 1397–1417.